Deletion of Both Rab-GTPase-Activating Proteins TBC1D1 and TBC1D4 in Mice Eliminates Insulin- and AICAR-Stimulated Glucose Transport

Chadt, Alexandra ; Immisch, Anja ; de Wendt, Christian ; Springer, Christian ; Zhou, Zhou ; Stermann, Torben ; Holman, Geoffrey D ; Loffing-Cueni, Dominique ; Loffing, Johannes ; Joost, Hans-Georg ; Al-Hasani, Hadi

Abstract: The Rab-GTPase-activating proteins TBC1D1 and TBC1D4 (AS160) were previously shown to regulate GLUT4 translocation in response to activation of AKT and AMP-dependent kinase. However, knockout mice lacking either Tbc1d1 or Tbc1d4 displayed only partially impaired insulin-stimulated glucose uptake in fat and muscle tissue. The aim of this study was to determine the impact of the combined inactivation of Tbc1d1 and Tbc1d4 on glucose metabolism in double-deficient (D1/4KO) mice. D1/4KO mice displayed normal fasting glucose concentrations but had reduced tolerance to intraperitoneally administered glucose, insulin, and AICAR. D1/4KO mice showed reduced respiratory quotient, indicating increased use of lipids as fuel. These mice also consistently showed elevated fatty acid oxidation in isolated skeletal muscle, whereas insulin-stimulated glucose uptake in muscle and adipose cells was almost completely abolished. In skeletal muscle and white adipose tissue, the abundance of GLUT4 protein, but not GLUT4 mRNA, was substantially reduced. Cell surface labeling of GLUTs indicated that RabGAP deficiency impairs retention of GLUT4 in intracellular vesicles in the basal state. Our results show that TBC1D1 and TBC1D4 together play essential roles in insulin-stimulated glucose uptake and substrate preference in skeletal muscle and adipose cells.

DOI: https://doi.org/10.2337/db14-0368

DB14-0368-Revised (**R3**)

Deletion of both Rab-GTPase activating proteins TBC1D1 and TBC1D4 in mice eliminates insulin- and AICAR-stimulated glucose transport

Alexandra Chadt[1,2], Anja Immisch[3], Christian de Wendt[1], Christian Springer[1], Zhou Zhou[1], Torben Stermann[1], Geoffrey D. Holman[4], Dominique Loffing-Cueni[5], Johannes Loffing[5], Hans-Georg Joost[2,3] and Hadi Al-Hasani[1,2§]

[1]German Diabetes Center, Leibniz Center for Diabetes Research at the Heinrich-Heine-University Düsseldorf, Germany; [2]German Center for Diabetes Research (DZD); [3]German Institute for Human Nutrition, Potsdam, Germany; [4]Department of Biology and Biochemistry, University of Bath, Bath, United Kingdom; [5]Institute of Anatomy, University of Zurich, Zurich, Switzerland.

[§]Corresponding author:
Hadi Al-Hasani
Institute for Clinical Biochemistry and Pathobiochemistry
German Diabetes Center, Leibniz Center for Diabetes Research at the Heinrich-Heine-University Düsseldorf
Auf'm Hennekamp 65
40225 Düsseldorf
Germany
tel/fax +49-211-3382-240/430
hadi.al-hasani@ddz,uni-duesseldorf.de

Running title: Insulin action in *Tbc1d1*/*Tbc1d4*- double-deficient mice
Word count: 4951
Figures: 8

Diabetes Publish Ahead of Print, published online September 23, 2014

Abstract

Previously, the Rab-GTPase activating proteins TBC1D1 and TBC1D4 (AS160) were shown to regulate GLUT4 translocation in response to activation of AKT and AMP-dependent kinase. However, knockout mice lacking either *Tbc1d1* or *Tbc1d4* displayed only partially impaired insulin-stimulated glucose uptake in fat and muscle tissue. The aim of this study was to determine the impact of the combined inactivation of *Tbc1d1* and *Tbc1d4* on glucose metabolism in double-deficient (D1/4KO) mice. D1/4KO mice displayed normal fasting glucose levels but had reduced tolerance to intraperitoneally administered glucose, insulin and AICAR, respectively. D1/4KO mice showed reduced respiratory quotient, indicating increased use of lipids as fuel. Consistently, D1/4KO mice showed elevated fatty acid oxidation in isolated skeletal muscle whereas insulin-stimulated glucose uptake in muscle and adipose cells was almost completely abolished. In skeletal muscle and white adipose tissue, the abundance of GLUT4 protein but not GLUT4 mRNA was substantially reduced. Cell surface labeling of glucose transporters indicated that RabGAP-deficiency impairs basal retention of GLUT4 in the basal state. Our results show that TBC1D1 and TBC1D4 together play essential roles in insulin-stimulated glucose uptake and substrate preference in skeletal muscle and adipose cells. (187 words)

Introduction

In skeletal muscle and adipose cells, insulin stimulation leads to a rapid and reversible redistribution of GLUT4 glucose transporters from intracellular vesicles to the cell surface (1; 2). The two related Rab–GTPase-activating proteins TBC1D1 and TBC1D4 (AS160) are phosphorylated in response to insulin, AMP-activated protein kinase (AMPK), and exercise/muscle contraction and have been implicated in playing important roles in regulating

the translocation of GLUT4 (3-9). By positional cloning, we previously identified a naturally occurring loss-of-function mutation in *Tbc1d1* as an obesity suppressor in the lean, diabetes-resistant SJL mouse strain (10). In humans, mutations in *TBC1D4* (R363X) and *TBC1D1* (R125W) have been linked to severe postprandial hyperinsulinemia and obesity, respectively (11-13). TBC1D4 is found mainly in the heart, adipose tissue and oxidative muscle fibers whereas TBC1D1 is predominantly expressed in glycolytic skeletal muscle and is nearly absent from fat tissue (10; 14; 15). Both TBC1D1 and TBC1D4 display a similar domain architecture that includes two N-terminal phosphotyrosine-binding (PTB) domains and a Rab-GTPase activating (GAP) domain. The latter is believed to control the activation state of RabGTPases by converting them from the active, GTP-bound state into the inactive GDP-bound state. Several lines of evidence suggest that the GAP domains in TBC1D1 and TBC1D4 directly regulate the activity of an overlapping set of Rab-GTPases, thereby controlling the subcellular targeting and transport activity of GLUT4 (7). So far, Rab2, Rab8b, Rab10 and Rab14 have been identified as substrates for recombinant GAP domains of TBC1D1 and TBC1D4 *in vitro* (4; 16), but the significance of these findings for GLUT4 translocation in adipose and muscle cells *in vivo* remains to be further investigated. Moreover, the PTB domains may also be involved in signaling of TBC1D1/TBC1D4 (17-19). Previous studies in isolated L6 muscle cells and 3L3-L1 adipocytes have demonstrated that ablation of either *Tbc1d1* or *Tbc1d4*, or overexpression of mutated proteins resulted in reduced insulin-stimulated translocation of GLUT4 (20-22). However, knockout mice lacking either *Tbc1d1* (15; 23) or *Tbc1d4* (14; 24) displayed only tissue-specific impairments of insulin-stimulated glucose uptake and rather minor alterations in glycemic control, indicating a substantial level of redundancy in expression and signaling.

The aim of this study was to determine the impact of the combined inactivation of *Tbc1d1* and *Tbc1d4* on glucose metabolism. Therefore, we characterized energy- and substrate metabolism of *Tbc1d1/Tbc1d4*- double-deficient mice. Our results demonstrate that both

TBC1D1 and TBC1D4 operate in concert and play essential roles in insulin-stimulated glucose uptake and substrate preference in skeletal muscle.

Material & Methods

Materials – Radiochemicals ([9,10(n)-^{3}H]-Palmitic acid; 2-[1,2-^{3}H(N)]-Deoxy-D-glucose, [1-^{14}C]-D-Mannitol and [^{14}C]-D-Glucose (U) were purchased from Hartmann Analytic, Braunschweig, Germany. Human recombinant insulin Actrapid HM Penfill from Novo Nordisk Pharma GmbH (Mainz, Germany) was used throughout the experiments. Collagenase (type I) was from Worthington Biochemical Corporation, Lakewood, NJ, USA. AICAR (5-Aminoimidazole-4-carboxamide ribonucleotide) was purchased from Enzo Life Sciences, Lörrach, Germany. Antibodies against TBC1D1 and GLUT4 were described previously (10). Antibodies against AKT, pAKT (Ser473), AMPKα, pAMPK (Thr172), and PCK2, Glycogen synthase and GSK3α were from Cell Signaling, Danvers, MA, USA. Antibodies against PCK1 were from Abcam, Cambridge, UK, Antibodies against TBC1D4 were from Millipore, Temecula, CA, USA, GAPDH Antibodies were from Ambion, Austin, TX, USA. Antibodies against IRAP and GLUT1 were a generous gift from Dr. Susanna Keller (University of Virginia, VA, USA) and Dr. Annette Schürmann (German Institute of Human Nutrition, Germany), respectively.

Experimental animals – Recombinant congenic *Tbc1d1*-deficient C57BL/6J mice (whole-body D1KO) were described previously (10). Mice with targeted deletion of *Tbc1d4* (whole-body D4KO) were obtained from TIGM (Texas A&M Institute for Genomic Medicine, Houston, TX, USA) and backcrossed to the D1KO strain using a microsatellite marker-assisted ("speed congenics") selection (25). Hererozygous D1KO/D4KO mice (>97.5% congenic with C57BL/6J were then intercrossed to generate the four experimental genotypes: Wildtype (WT), D1KO, D4KO, and *Tbc1d1/Tbc1d4* double-deficient D1/4KO. Animals

were kept in accordance with the NIH guidelines for the care and use of laboratory animals and all experiments were approved by the Ethics Committee of the State Ministry of Agriculture, Nutrition and Forestry (States of Brandenburg and North Rhine-Westphalia, Germany). Three to six mice per cage (Macrolon type III) were housed with *ad libitum* access to food and water at a temperature of 22°C and a 12 h light-dark cycle (lights on at 6 a.m.). After weaning at the age of 19-21 days, animals received a standard chow with 19% (wt/wt) protein (23 cal%), 3.3% fat (8 cal%) and 54.1% carbohydrates (69 cal%) containing 3.06 kcal/g energy (V153x R/M-H, Ssniff, Soest, Germany).

Genotyping – Isolation of DNA from mouse tail tips was performed with the InViSorb Genomic DNA Kit II (Invitek, Berlin, Germany). Genotyping of mice was performed by PCR with three primers for the *Tbc1d4* knockout (Fwd: 5'-AGTAGACTCAGAGTGGTCTTGG-3', Rev-KO: 5'-GTCTTCCGACTCCATATTTGC-3', Rev-WT: 5'-GCAGCGCATCGCCTTCTATC-3') and primers for D1KO mice as described (10).

RNA extraction, cDNA synthesis and quantitative real-time PCR – RNA extraction and cDNA synthesis was performed as described (10). Real-time PCR was performed with an Applied Biosystems 7500 Fast Real-Time PCR-System using TaqMan PCR probes (Applied Biosystems, Foster City, CA, USA) for *Tbc1d1*, *Tbc1d4*, *Slc2a4* and data were normalized to *Actb* according to the ΔCt method (26).

Analysis of body weight, body composition– Body weight was measured with an electronic scale (Sartorius, Göttingen, Germany), body composition was analyzed with a nuclear magnetic resonance spectrometer (Echo MRI, Houston, TX, USA).

Indirect calorimetry – Animals were placed in individual cages and respiratory quotient (RQ) was measured after an adaption phase of 24 h by indirect calorimetry as described (23). Rates of oxygen consumption (VO_2) and carbon dioxide production (VCO_2) were monitored for

23 h at 22°C at a flow rate of 30 l/min. Animals had free access to water, and food was removed during daytime (6 a.m. – 6 p.m.). Whole body carbohydrate and fat oxidation rates (g/min) were calculated using the following equations: carbohydrate oxidation rate = 4.585 × VCO_2 (l/min) − 3.226 × VO_2 (l/min); fat oxidation rate = 1.695 × VO_2 (l/min) − 1.701 × VCO_2 (l/min) (27).

Tolerance tests – For glucose tolerance tests, sterile glucose (2 g/kg body weight, 20% solution) was injected intraperitoneally (i.p.) into fasted (16 h) animals. For insulin- and AICAR-tolerance tests, non-fasted mice were injected i.p. either with Insulin (1 IU/kg body weight) or AICAR (250 mg/kg body weight), and blood samples were taken at 0, 15, 30, 60 (i.p. ITT and ATT) and additionally at 120 min (i.p.GTT) from the tail tip. Blood glucose was determined with a glucometer (Contour, Bayer, Leverkusen, Germany). Plasma insulin was measured with ELISA (Insulin Mouse Ultrasensitive ELISA, DRG, Germany).

Determination of free fatty acids, triglycerides and glycogen – 30 mg frozen tissue (liver and *skeletal* muscle) was pestled and analyzed using the Triglycerides (TRIGS) GPO-PAP Kit (Randox, Crumlin, UK) according to the manufacturer's guidelines. Muscle homogenates were tested negatively for adipocyte contamination (Supplementary Figure 1). Glycogen was determined by the amyloglucosidase method (28). Tissue homogenates were incubated with 30%KOH (wt/vol) at 100°C for 30 minutes, respectively. Subsequently, samples were supplemented with acetic acid and assay buffer containing sodium acetate and amyloglucosidase and incubated 3 h at 37°C. Glucose was then measured enzymatically by a glucose oxidase-based colorimetric detection kit (Glucose liquicolor, Human, Taunusstein, Germany) according to the manufacturer's instructions.

Analysis of glucose uptake in adipocytes – Primary adipose cells were isolated by collagenase digestion of epididymal fat pads from 12-16 week old male mice, and basal and insulin-stimulated uptake of [^{14}C]glucose was performed as described (29). Briefly, freshly

isolated adipose cells (30) were incubated in Krebs-Ringer bicarbonate HEPES buffer, pH 7.4, 200 nM adenosine containing 5% bovine serum albumin without and without 120 nM insulin for 30 min before measurement of [^{14}C]glucose uptake. After 30 min, the cells were spun through dinonylphtalate oil (Merck, Darmstadt, Germany) to remove excess label, and the cell-associated radioactivity was determined by scintillation measurement. The resulting counts were normalized to the lipid weight of the samples (29). Measurements were performed in quadruplicate.

Analysis of glucose uptake and fatty acid oxidation in isolated skeletal muscles – [^{3}H]2-deoxyglucose uptake in intact isolated skeletal muscles was performed as described (10). *Extensor digitorum longus* (*EDL*) and *Soleus* muscles were removed from anesthetized (500 mg/kg Avertin (2,2,2-Tribromoethanol, TBE; i.p. Injection)) mice. Animals were then euthanized by heart puncture under anesthesia. Isolated muscles were incubated for 30 min at 30°C in vials containing pre-oxygenated (95% O_2/ 5% CO_2) Krebs-Henseleit buffer (KHB) containing 5 mM HEPES and supplemented with 5 mM glucose and 15 mM mannitol. All incubation steps were conducted under continuous gassing (95% O_2/ 5% CO_2) at 30°C and slight agitation. After recovery, muscles were transferred to new vials and incubated for 30 min in KHB/ 5 mM HEPES/ 15 mM mannitol/ 5 mM glucose under basal condition or in the presence of 120 nM insulin or 2 mM AICAR, respectively, throughout the duration of the experiment. Then, muscles were incubated for 10 minutes in in KHB/ 20 mM mannitol under basal condition or in the presence of 120 nM insulin or 2 mM AICAR, respectively, before being transferred to the radioactive glucose transport incubation. After 20 min incubation in the presence of 1 mM [^{3}H]2-deoxy-glucose and 19 mM [^{14}C]mannitol, muscles were immediately frozen in liquid nitrogen and stored at -80°C. Cleared protein lysates were used to determine incorporated radioactivity by scintillation counting. The counts from [^{14}C]mannitol were used to correct for the extracellular space.

To assess palmitate oxidation, *EDL* and *Soleus* muscles were incubated in pre-gassed KHB containing 15 mM mannitol, 5 mM glucose, 3.5% fatty acid-free BSA, [^{3}H]palmitate and 600 μM unlabeled palmitate with or without 2 mM AICAR at 30°C for 2 h. After absorption of fatty acids to activated charcoal, fatty acid oxidation was determined by scintillation measurement of tritiated water.

Cell surface photolabeling of GLUT4 – Affinity-photolabeling of glucose transporters using the Bio-LC-ATB-BGPA compound was performed as described (31). Following a 4h fasting period, mice were anesthetized and *EDL* and *Soleus* muscles were removed. Muscles were incubated in glass vials in pre-oxygenated KHB buffer containing 0.1% BSA, 2 mM Pyruvate and 18 mM Mannitol for 30 minutes at 30°C. After recovery, 400 μM Bio-LC-ATB-BGPA was added and muscles were incubated with (120 nM) or without insulin at 18°C for 8 minutes in the dark. After UV irradiation (6 min, 354 nm, 4°C) muscles were immediately frozen in liquid nitrogen. Recovery of photochemically biotinylated proteins from muscle lysates using streptavidin beads (Pierce, Rockford, IL, USA) was performed as described, and total and labeled GLUT4 was determined by Western Blots analysis.

SDS-PAGE and Western Blot – Tissues were homogenized (20 mM Tris, 150 mM NaCl, 1 mM EGTA, 1 mM EDTA, 1% (v/v) Triton-X-100, 1 mM Na_3VO_4, 1 mM β-glycerolphosphate, 1 mM NaF, 2.5 mM $Na_4P_2O_7$ and a proteinase inhibitor and a phosphatase inhibitor cocktail (Complete and PhosSTOP, Roche, Mannheim, Germany) and centrifuged for 10 min at 16.000 rcf at 4°C. Protein content was determined from the supernatant with the BCA Protein Assay Kit (Pierce, Rockford, IL, USA). Immunoblotting and detection was performed with ECL Western blot detection analysis system (GE Healthcare, Buckinghamshire, UK) as described (23).

Statistics – Data are reported as means ± SEM. Significant differences were determined by one-way or two-way ANOVA (*post-hoc test*, Bonferroni multiple comparison test) or paired

two-tailed Student's t-test as indicated in the Figure legends. Values of $p<0.05$ were considered statistically significant.

Results

Tbc1d1/Tbc1d4-double-deficient mice show only marginal differences in body weight, body fat

We crossbred mice deficient in *Tbc1d1* (whole-body D1KO) with conventional *Tbc1d4* knockout animals (whole-body D4KO) to yield *Tbc1d1/Tbc1d4* double-deficient (D1/4KO) mice on a C57BL/6J background. In all tissues analyzed, the abundance of TBC1D4 was not altered in *Tbc1d1*-deficient mice (Fig. 1A-C and Supplementary Figure 2). Equally, TBC1D1 protein was not changed in mice deficient in *Tbc1d4* (Fig. 1A-C, Supplementary Figure 2). Male D1KO, D4KO and D1/4KO mice and wildtype littermates (WT) were raised on a standard diet (8% calories from fat), and body weight and body composition were measured every 3 weeks until week 21. On a standard diet, D1KO, D4KO and D1/4KO mice showed a lower body weight and a tendency towards reduced fat mass whereas lean mass was not different compared to WT controls (Fig. 1D-F).

Tbc1d1/Tbc1d4-double-deficient mice show impaired glucose, insulin and AICAR tolerance

Plasma glucose and insulin levels were determined in standard-diet fed male D1KO, D4KO and D1/4KO mice and wild-type littermates. D1KO and D4KO mice showed normal plasma glucose and insulin levels in both postprandial and fasted states (Fig. 2A, B). In contrast, postprandial glucose levels were decreased in D1/4KO mice (WT *vs*. D1/4KO*:* 7.31±0.18 *vs.* 6.34±0.24 mmol/l; $p<0.01$) whereas fasting glucose levels were normal. Moreover, fed and fasted plasma triglycerides as well as free fatty acids in plasma were not different between

the genotypes, respectively (Supplementary Figure 3). In order to investigate whole-body glycemic control of the animals we performed intraperitoneal tolerance tests for glucose (i.p.GTT), insulin (i.p.ITT), and AICAR (i.p.ATT). D1KO and D4KO mice showed normal blood glucose levels, as well as normal plasma insulin levels during the i.p.GTT (Fig. 2C and 2D). In contrast, *D1/4KO* mice displayed markedly impaired glucose tolerance while insulin levels were normal (Fig. 2C and 2D). Similarly, D1KO and D4KO mice showed normal blood glucose levels in response to intraperitoneal injection of insulin (i.p.ITT) while D1/4KO mice displayed substantially impaired insulin tolerance (Fig. 2E). Lastly, D4KO retained normal blood glucose levels in response to intraperitoneal injection of AICAR (i.p.ATT) while both D1KO and D1/4KO mice had significantly impaired AICAR tolerance (Fig. 2F).

Tbc1d1/Tbc1d4 depletion increases fatty acid oxidation in vivo

We investigated whole-body substrate utilization in standard-diet fed male D1KO, D4KO and D1/4KO mice and WT littermates. At the age of 13 weeks, animals were placed in metabolic cages and indirect calorimetry was conducted for 24 h. On a standard diet, D1KO, D4KO and D1/4KO mice showed a substantial reduction in respiratory quotient (RQ) compared to wild-type controls during the dark phase (Fig. 3A, B). Whole-body fat oxidation rates were increased substantially whereas whole-body carbohydrate oxidation rate was significantly reduced only in D1/4KO mice (Fig. 3C, D).

Glucose uptake is impaired in skeletal muscle from Tbc1d1/Tbc1d4-double-deficient mice

In order to determine the specific contribution of TBC1D1 and TBC1D4 to glucose uptake in skeletal muscle, *EDL* and *Soleus* muscles from 16-week-old male mice were isolated and assayed for insulin- and AICAR-stimulated uptake of 2-deoxyglucose as described in the methods section. In glycolytic *EDL* muscle, basal 2-deoxyglucose uptake was not

significantly different between the genotypes (Fig. 4A). In contrast, glucose uptake in response to insulin was substantially impaired in *EDL* muscles from D1KO and D1/4KO mice whereas glucose uptake in *EDL* muscle from D4KO mice was normal (Fig. 4A). Similarly, AICAR-stimulated uptake of 2-deoxyglucose was markedly decreased in *EDL* muscles from D1KO and D1/4KO mice but not in *EDL* muscles from D4KO mice (Fig. 4B). In oxidative *Soleus* muscle, basal glucose uptake was also not different between the genotypes (Fig. 4C). However, insulin-stimulated glucose uptake was markedly reduced in *Soleus* muscles from D4KO and D1/4KO mice whereas glucose uptake in the *Soleus* muscle from D1KO mice was normal (Fig. 4C). Again, AICAR-stimulated glucose uptake was decreased correspondingly (Fig. 4D).

Glucose uptake is impaired in WAT from Tbc1d1/Tbc1d4-double-deficient mice

We determined the impact of *Tbc1d1/Tbc1d4*-deficiency on glucose uptake in isolated white adipose cells. Adipose cells from 16week-old male mice were isolated by collagenase digestion and assayed for insulin-stimulated uptake of ^{14}C-D-glucose as described in the methods section. In basal adipose cells, glucose uptake was not different between the genotypes (Fig. 4E). However, insulin-stimulated glucose uptake was markedly reduced in adipose cells from D4KO and D1/4KO mice whereas glucose uptake in cells from D1KO mice was normal (Fig. 4E).

Tbc1d1/Tbc1d4-deficiency has no impact on signaling of AKT2 and AMPK

We next investigated whether insulin or AMPK signaling were impaired in skeletal muscle from D1KO, D4KO, and D1/4KO mice. Basal and insulin (120 nM; 60 min) stimulated *EDL* muscle was homogenized, and AKT expression and phosphorylation of AKT^{Ser473} was analyzed by Western blot. In addition, basal and AICAR-stimulated (2 mM; 60 min) *Soleus* muscle were homogenized, and both AMPK expression and phosphorylation of AMPK^{Thr172}

were analyzed by Western blot. Quantitative assessment of replicate skeletal muscle samples revealed that neither expression nor phosphorylation of AKT or AMPK differed between genotypes (Fig. 4F). Moreover, we found no evidence for compensatory changes in phosphorylation of TBC1D1 and TBC1D4 (TBC1D1^{Ser237}, TBC1D4^{Thr588}, PAS phosphoylation) in insulin-stimulated skeletal muscle from knockouts (Supplementary Figure 4)

Tbc1d1/Tbc1d4-deficiency results in elevated FAO in skeletal muscle

To determine the role of TBC1D1 and TBC1D4 in lipid utilization in skeletal muscle, *EDL* and *Soleus* muscles from 16-week-old male mice were isolated and assayed for basal and AICAR-stimulated oxidation of palmitate as described in the methods section. In glycolytic *EDL* muscle, basal palmitate oxidation was increased substantially (~2-fold) in mice deficient in either *Tbc1d1, Tbc1d4* or both (Fig. 5A). In intact isolated *EDL* muscle from control animals, AICAR stimulation led to a >2-fold increase in FAO (Fig. 5A). In contrast, in *EDL* muscle from D1KO, D4KO and D1/4KO mice, the rates of FAO were not further increased in response to AICAR (Fig. 5A). In oxidative *Soleus* muscle, basal palmitate oxidation was markedly increased (~1.4-fold) in mice deficient in *Tbc1d1* whereas no changes in FAO were observed in mice lacking either *Tbc1d4* or double-deficient mice (Fig. 5B). For AICAR-stimulated FAO in *Soleus* muscle, no significant differences were observed between the genotypes (Fig. 5B). The copy numbers of mitochondrial DNA (mtDNA) in *Gastrocnemius* muscle were not different between genotypes (Supplementary Figure 5A). However, citric acid synthase (CS) activity was moderately elevated in *Gastrocnemius* muscle from D1KO mice (Supplementary Figure 5B).

Abundance of GLUT4 is reduced in skeletal muscle and WAT from Tbc1d1/Tbc1d4-deficient mice

In skeletal muscle, the mRNA levels for GLUT4 were not different between the genotypes (Supplementary Fig. 6). To further examine the mechanism for the reduced insulin- and AICAR-stimulated glucose uptake in skeletal muscle and adipose cells, tissues from 16-week-old male mice were homogenized and the abundance of GLUT4 protein was determined by Western blot analysis. D1KO mice displayed strongest reduction (~40-50%) in GLUT4 content in EDL and *Tibialis anterior* (*TA*) muscle, whereas the abundance of GLUT4 was reduced by only ~30% in *Quadriceps* muscle (Fig. 6A, B, E). In D4KO mice, GLUT4 was reduced to ~75% in *Soleus* muscle and to ~60% in WAT (Fig. 6C, F). Correspondingly, D1/4KO mice showed reduced GLUT4 content in all tissues analyzed. The abundance of the GLUT4-associated aminopeptidase IRAP (32) was also significantly reduced in *EDL* and *Soleus* muscle from D1/4KO mice (Supplementary Fig. 7).

RabGAP-deficiency impairs basal retention of GLUT4 in intracellular vesicles

We investigated alterations in the subcellular distribution of GLUT4 by using bio-LC-ATB-BGPA, a cell surface impermeant bis-glucose photolabeling reagent (31). Intact isolated EDL and soleus muscles from D1KO mice were incubated with bio-LC-ATB-BGPA in the absence or presence of insulin as described in methods. After UV irradiation to cross-link the photoactivated diazirine group of bio-LC-ATB-BGPA to cell surface-localized glucose transporters, photolabeled GLUT4 was recovered from cell membranes by using streptavidin-agarose and quantified by immunoblotting with GLUT4 antibodies. Compared to the wildtype controls, the amount of photolabeled cell surface GLUT4 was significantly reduced in insulin-stimulated EDL muscles (Fig. 7A). In contrast, basal levels of photolabeled cell surface GLUT4 from *Tbc1d1*-deficient EDL were not different from controls. In soleus muscle from D1KO mice however, the levels of photolabeled GLUT4 was similar in the basal and insulin -stimulated states, respectively (Fig. 7B). When the amount of total GLUT4

is taken into account, the proportion of GLUT4 at the cell surface is increased in EDL but not in soleus muscle from D1KO mice (Fig. 7C, D). Similar changes occur in D4KO mice (24).

***Tbc1d1/Tbc1d4*-deficiency reduces glycogen and increases triglyceride levels in the liver.**

We investigated the impact of *Tbc1d1/Tbcd4* deficiency on the content of triglycerides and glycogen in skeletal muscle and liver from mice fasted for 4 h. Hepatic glycogen levels were substantially decreased in D1KO, D4KO and D1/4KO mice when compared to WT controls (Fig. 8A). In contrast, fasting glycogen was increased in *Quadriceps* muscle of D1/4KO mice compared to WT controls (Fig. 8B). There was a trend for increased glycogen in *Gastrocnemius* muscle in D1/4KO mice, but the difference was not significant (Fig. 8B). Abundance of glycogen synthase (GS) and phosphorylation (Ser^{641}) were not significantly different between the genotypes in liver and muscle (Supplementary Figure 8). Also, no differences in abundance of GSK3α and phosphorylation (Ser^{21}) were observed in liver and muscle (Supplementary Figure 8). Hepatic triglyceride levels were increased in D1KO, D4KO and D1/4KO mice (Fig. 8C) whereas triglycerides in muscle were not changed (Fig. 8D). Expressions of both forms of the gluconeogenic enzyme phosphoenolpyruvate carboxykinase, *Pck1* and *Pck2*, were increased in liver from D1KO, D4KO and D1/4KO mice (Fig. 8E, F).

Discussion

In this study, we investigated the impact of the combined inactivation of *Tbc1d1* (D1KO) and *Tbc1d4* (D4KO) on glucose and lipid metabolism in *Tbc1d1/Tbc1d4*- double-deficient (D1/4KO) mice. Our results demonstrate that both RabGAPs play critical roles in GLUT4 trafficking, glucose and lipid metabolism in muscle and adipose tissue.

On a standard diet, D1/4KO mice showed moderately reduced body weight and a trend towards reduced fat mass. Moreover, D1/4KO mice showed a reduced RQ which resulted from a substantial increase in whole-body fatty acid oxidation and decreased use of carbohydrates as fuel. Both D1KO and D4KO mice displayed a similar reduction in body weight and RQ, suggesting that *Tbc1d1* and *Tbc1d4* may both contribute to energy substrate preference in the animals. In a previous study, animals expressing a signaling-deficient *Tbc1d4*-(T642A) mutant (33) also displayed reduced body weight, whereas *Tbc1d4* knockout mice generated by Nestin-Cre/Lox-mediated deletion of the gene showed no significant change in body weight (14). In contrast, *Tbc1d1* deficiency was found to substantially reduce body weight and RQ in high-fat diet-fed obese mice, indicating a possible interaction of the gene with dietary fat and/or obesity (10).

Similar to the single knockouts, D1/4KO mice had normal fasting glucose levels. However, in contrast to D1KO and D4KO animals, D1/4KO mice displayed markedly impaired tolerance to glucose, insulin and AICAR, indicating an important role of both RabGAPs in glucose disposal *in vivo*. Thus, the impact of a single RabGAP knockout on glycemic control, i.e. D1KO and D4KO, appears to be largely compensated by the residual RabGAP activity of the functioning gene whereas inactivation of both RabGAPs leads to a pronounced impairment of glucose disposal. Interestingly, D1KO mice had reduced AICAR tolerance compared to D4KO animals, indicating an increased relevance of TBC1D1 in the AICAR response. This might reflect tissue specific differences in RabGAP abundance and/or AICAR sensitivity of the RabGAPs. The reduced postprandial glucose levels in D1/4KO mice could be related to a proposed function of the RabGAPs in insulin secretion (34; 35). However, we did not observe genotype-specific differences in circulating insulin levels.

In mice, *Tbc1d1* is predominantly expressed in glycolytic muscle fibers whereas *Tbc1d4* is expressed more strongly in oxidative muscle and in adipose cells (14; 23). Consistent with

the tissue-specific expression profile of both RabGAPs, insulin-stimulated glucose uptake in D1KO mice was substantially reduced in intact isolated *EDL* muscle, but normal in *Soleus* muscle and isolated adipose cells. Conversely, D4KO mice showed severely impaired insulin-stimulated glucose uptake in *Soleus* muscle and adipose cells whereas glucose uptake was normal in *EDL* muscle. The combined ablation of both RabGAPs in D1/4KO mice essentially resulted in elimination of insulin- and AICAR- stimulated glucose uptake in *EDL* and *Soleus* muscle, and in a substantial reduction of insulin-stimulated glucose uptake in adipose cells. However, deletion of one of the RabGAPs (e.g. *Tbc1d1* in *EDL*, *Tbc1d4* in *Soleus* and WAT) is sufficient to abolish insulin and AICAR-stimulated glucose uptake without any further reduction in glucose transport in these tissues in the double knockout mice. In D1KO mice GLUT4 associated glucose transport is clearly deficient in glycolytic muscle and yet GTT and ITT responses are normal. This suggests that glycolytic muscle types alone are not essential for maintenance of whole animal glucose homoeostasis, possibly due to a background maintenance of TBC1D4 activity and normal glucose transport activity in non-glycolytic muscle. Consistent with these findings, previous studies of GLUT4-deficient mice also demonstrated substantial compensation for reduced glucose transport in muscle and adipose tissue by altering hepatic fuel metabolism and increasing utilization of fatty acids (36). Thus, taken together, *Tbc1d1* and *Tbc1d4* play an essential role in insulin- and AICAR-stimulated glucose uptake in both skeletal muscle and adipose cells, respectively.

The reduced glucose uptake in response to insulin and AICAR was paralleled by considerable reduction in GLUT4 abundance in muscle and adipose cells, respectively. Because the mRNA levels of GLUT4 were unaltered in the knockout mice, the decrease in glucose transporters is likely the result of posttranslational events and may reflect missorting of the protein, presumably due to altered function of one or more Rabs downstream of

TBC1D1/TBC1D4 (14; 23; 24; 37). Consistent with a defect in protein sorting, the abundance of the insulin-regulated aminopeptidase IRAP, a resident protein of GLUT4 vesicles (38; 39), binding partner of TBC1D4 (40) and potential regulator of GLUT4 sorting (41), was also significantly reduced in both *EDL* and *Soleus* muscle from D1/4KO mice.

Previous studies have shown that in adipose cells and skeletal muscle basal glucose transport is strongly correlated with the abundance of GLUT4 protein. Deletion of GLUT4 in these tissues led to a profound reduction in basal glucose transport whereas overexpression of GLUT4 resulted in a substantial increase in basal uptake of glucose into the cells (42-45). In contrast, in skeletal muscle and adipose cells from D1KO, D4DO and D1/4KO mice, basal glucose transport was normal despite substantially reduced abundance of cellular GLUT4 protein. Thus, the dissociation of basal glucose transport and GLUT4 abundance mice suggests that lack of RabGAPs leads to a redistribution of GLUT4 from intracellular compartments to the cell surface in the basal state. We therefore investigated the subcellular distribution of GLUT4 by cell surface photolabeling of the protein in *EDL* and Soleus muscle from D1KO mice and compared the surface level with the total GLUT4 level. Consistent with the glucose transport data, the amount of basal cell surface GLUT4 in EDL muscle of D1KO mice was comparable with wild type despite lower abundance of total GLUT4. Thus, in unstimulated D1KO cells, a higher proportion of GLUT4 was present on the cell surface. In the insulin stimulated state, both glucose uptake and cell surface GLUT4 were equally reduced compared with wild-type, indicating that the fraction of GLUT4 that is present on the plasma membrane in insulin-stimulated cells is relatively normal. Thus while it is not known at what stage in GLUT4 trafficking TBC1D1 and TBC1D4 participate at the molecular level, our findings are consistent with the RabGAPs being involved in intracellular retention of GLUT4 vesicles in the basal state (22; 46).

Consistent with the reduction in RQ, D1KO, D4KO and D1/4KO mice exhibited elevated basal FAO in *EDL* muscle. In the oxidative *Soleus* muscle, FAO was only elevated in D1KO mice and not further increased by AICAR stimulation. Unexpectedly, *Soleus* muscle from D1/4KO mice did not show increased FAO despite the lack of TBC1D1, indicating that additional factors might be involved that modulate lipid oxidation in this type of muscle. In contrast, D1KO, D4KO and D1/4KO mice had equally increased levels of FAO in glycolytic *EDL* muscle which also was not further increased by AICAR. Thus, in glycolytic muscle inactivation of each RabGAP equally contributes to the elevated FAO. Moreover, elevation of FAO is not directly related to impaired glucose uptake as *Tbc1d4* knockouts have normal glucose uptake but increased FAO in *EDL* muscle. The mechanism responsible for the elevated FAO in glycolytic skeletal muscle of RabGAP-deficient mice remains to be clarified. Previously we have shown that knockdown *Tbc1d1* in cultured skeletal muscle cells also increases fatty acid uptake and oxidation whereas overexpression of the gene has the opposite effect (10). However, overexpression of a RabGAP-deficient mutant, *Tbc1d1*-R941K, had no effect on fatty acid uptake and oxidation, indicating an involvement of Rab-GTPases in this process (10). Interestingly, knockout of both *Tbc1d1* and *Tbc1d4* did not exert additive effects on FAO in *EDL* muscle which suggests that both RabGAPs may regulate the same downstream target.

RabGAP-deficient D1/4KO mice phenocopy adipose- and muscle-specific GLUT4 knockout mice (AMGKO) as these animals show substantially reduced glucose uptake in response to insulin, and elevated use of lipids as energy source (36). In fact, the reduced abundance of GLUT4 at least in part explains the decreased glucose uptake in response to a stimulus. The inability to utilize glucose in muscle and adipocytes is associated with elevated hepatic trigycerides and reduced hepatic glycogen content, whereas fasting glycogen levels in skeletal muscle tend to be increased. While hepatic glycogen levels of AMGKO mice were

not reported, conversion of glucose to fatty acids in the liver was substantially increased in these animals (36). Consistent with our data, muscle specific GLUT4 knockout mice also displayed increased fasting glycogen content in skeletal muscle despite substantially reduced glucose uptake (47). A complex counterregulation of increased glycogen synthesis and decreased glycogen breakdown was proposed to explain this effect (47). We could not confirm a substantial increase in glycogen synthesis in skeletal muscle from fasted D1/4KO mice, however, the effect size might be larger in muscle completely lacking GLUT4. Thus, the mechanistic basis for the underlying tissue crosstalk remains to be further explored.

In summary, our results indicate that both RabGAPs play important roles in GLUT4 trafficking, glucose and lipid metabolism in muscle and adipose cells. So far, of the many Rab GTPases previously found to be associated with GLUT4-containing compartments (48; 49), only Rab8, Rab10 and Rab14 were identified as substrates for both TBC1D1 and TBC1D4 *in vitro,* and furthermore have been implicated to play roles in trafficking of GLUT4 *in vivo* (50-53). Future studies are required to investigate the specific contribution of the Rabs to the regulation of metabolic flexibility.

Acknowledgements

We thank Carolin Borchert, Diana Schulze, Ines Grüner, Angelika Horrighs, Anette Kurowski, Ilka Römer, Annette Schober, Antonia Osmers and Jennifer Schwettmann for expert technical assistance, and Susanna Keller and Annette Schürmann for generously providing antibodies. This work was supported by the Ministry of Science and Research of the State of North Rhine-Westphalia (MIWF NRW) and the German Federal Ministry of Health (BMG), and funded in part by grants from the Deutsche Forschungsgemeinschaft (GRK1208, AL452/4-1), the German Academic Exchange Service (DAAD) for G.D.H., and

the EFSD/Lilly European Diabetes Research Program, and the Swiss National Science Foundation (310000-122243/1, 310030-143929/1).

Duality of interest

None of the authors has a duality of interest to declare.

Author Contributions

A.C. and H.A.-H. conceived the experiments, analyzed data, and wrote the manuscript. A.C., A.I., C.d.W., C.S., Z.Z., T.S., and D.L-C. performed the experiments and contributed to data analysis. A.C., H.A.-H., J.L., G.D.H. and H.-G.J. contributed to discussion and reviewed and edited the manuscript. H.A.-H. is the guarantor of this work and, as such, had full access to all of the data in the study and takes responsibility for the integrity of the data and the accuracy of the data analysis.

Figure legends

Figure 1: Disruption of *Tbc1d1* and *Tbc1d4* moderately reduces body weight. A, Western Blot of TBC1D1 and TBC1D4 in *Tibialis anterior* (*TA*) muscle and white adipose tissue (WAT) from *Tbc1d1*-deficient (D1KO), *Tbc1d4*-deficient (D4KO) and double-deficient (D1/4KO) mice. B, Quantification of TBC1D1 and TBC1D4 protein abundance determined by Western Blot analysis in glycolytic *EDL* (*Extensor digitorum longus*) muscle and C, oxidative *Soleus* muscle. Data presented as mean ±SEM, n=3-8. D, Body weight development of male D1KO, D4KO and D1/4KO. E, Body fat development. F, Lean mass. Data presented as mean ±SEM, n=11-22. $^{*}p<0.05$, $^{**}p<0.01$, WT vs. D1KO, D4KO, D1/4KO (one-way ANOVA).

Figure 2: Deficiency in *Tbc1d1*/*Tbc1d4* impairs glucose, insulin and AICAR tolerance. A, Blood glucose and B, plasma insulin levels of *Tbc1d1*-deficient (D1KO), *Tbc1d4*-deficient (D4KO) and double-deficient (D1/4KO) mice in the fed state and after 16h of fasting. Data presented as mean ±SEM, n=13-27. $^{*}p<0.05$, $^{**}p<0.01$, $^{***}p<0.001$, fed vs fasted (two-way ANOVA) and WT vs. D1/4KO (one-way ANOVA). Male mice aged 12-16 weeks were subjected to intraperitoneal (i.p.) tolerance tests for glucose (GTT), insulin (ITT), and AICAR (ATT). C, Blood glucose levels of D1KO, D4KO and D1/4KO mice after i.p. injection of glucose (2 mg/kg). D, Plasma insulin levels during i.p.GTT. E, Blood glucose levels during i.p.ITT (1 IU/ kg). F, Blood glucose levels during i.p.ATT (250 mg/kg). Data presented as mean ±SEM, n=8-16. $^{*}p<0.05$, WT vs. D1KO, D1/4KO (one-way ANOVA).

Figure 3: Deletion of *Tbc1d1* and *Tbc1d4* alters energy substrate preference. Male mice aged 12-16 weeks were subjected to indirect calorimetry. A, Respiratory quotient (RQ) of D1KO, D4KO and D1/4KO mice. B, Mean respiratory quotient (RQ). C, Whole-body carbohydrate oxidation (CHO). D, Whole-body fatty acid oxidation (FAO). Data presented as mean ±SEM, n=8-11. $^{*}p<0.05$, $^{**}p<0.01$, $^{***}p<0.001$,WT vs. D1KO, D4KO, D1/4KO (one-way ANOVA).

Figure 4: Lack of *Tbc1d1* and *Tbc1d4* impairs glucose uptake in skeletal muscle and adipose cells. Skeletal muscles and adipose cells from 16-week-old male mice and controls were isolated and assayed for glucose uptake. A, Insulin-stimulated [^{3}H]-deoxyglucose uptake in *Extensor digitorum longus* (*EDL*) muscle from D1KO, D4KO and D1/4KO mice (n=9-15). B, AICAR-stimulated [^{3}H]-deoxyglucose uptake in *EDL* muscle (n=6-11). C, Insulin-stimulated [^{3}H]-deoxyglucose uptake in isolated *Soleus* muscle (n=6-9). D, AICAR-stimulated [^{3}H]-deoxyglucose uptake in isolated *Soleus* muscle (n=6-11). E, Insulin-stimulated [^{14}C]-D-glucose (U) uptake in isolated adipocytes from epididymal WAT (n=4-6). F, Quantification of Western blot analyses of AKT and AMPK phosphorylation in isolated

EDL and *Soleus* muscles after *ex vivo* insulin and AICAR stimulation, respectively. *EDL*: Left panel, *Soleus*: Right panel (n=4-6). Data presented as mean ±SEM, $^{*}p<0.05$, $^{**}p<0.01$, $^{***}p<0.001$, basal vs insulin/AICAR (two-way ANOVA), and WT vs. D1KO, D4KO, D1/4KO (one-way ANOVA).

Figure 5: Deletion of *Tbc1d1* and *Tbc1d4* leads to elevated FAO in skeletal muscle. Skeletal muscles from 16-week-old male mice and controls were isolated and assayed for fatty acid oxidation as described in methods. A, AICAR-stimulated *ex vivo* [^{3}H]-palmitate oxidation in isolated *EDL* muscle from D1KO, D4KO and D1/4KO mice. B, AICAR-stimulated *ex vivo* [^{3}H]-palmitate oxidation in isolated *Soleus* muscle from D1KO, D4KO, and D4KO mice. Data presented as mean ±SEM, n=7-8. $^{*}p<0.05$, $^{**}p<0.01$, basal vs. AICAR (two-way ANOVA) , and WT vs. D1KO, D4KO, D1/4KO (one-way ANOVA).

Figure 6: Deficiency in *Tbc1d1* and *Tbc1d4* reduced abundance of GLUT4 in skeletal muscle and white adipose tissue. GLUT4 protein abundance was determined by Western Blot analysis of tissues from knockout mice and wildtype littermate controls. A, *Tibialis anterior* (*TA*) muscle. B, *Extensor digitorum longus* (*EDL*) muscle. C, *Soleus* muscle. D, *Quadriceps* muscle. E, *Gastrocnemius* muscle. F, White adipose tissue. Data presented as mean ±SEM, n=5-10. $^{*}p<0.05$, $^{**}p<0.01$, $^{***}p<0.001$, WT vs. D1KO, D4KO, D1/4KO (one-way ANOVA). G, H, Representative Western Blot analysis of TBC1D1, TBC1D4, GLUT1 and GLUT4 in *Extensor digitorum longus* (*EDL*) and *Soleus* muscle.

Figure 7: *Tbc1d1*-deficiency leads to subcellular redistributions of GLUT4.

Following a 4h fasting period, mice were anesthetized and *EDL* and *Soleus* muscles were removed. Muscles in the basal and insulin-stimulated states were cell surface labelled with impermeant Bio-LC-ATB-BGPA. Biotinylated proteins were recovered from muscle lysates using immobilized streptavidin beads and resolved by SDS-PAGE. Total and labelled cell

surface GLUT4 were determined by Western Blots analysis. The levels of cell surface GLUT4 were then compared without (A, B; *EDL* and *Soleus*, respectively; bands show recovered biotinylated GLUT4) or with correction for total GLUT4 (C, D; *EDL* and *Soleus*, respectively; bands show total GLUT4). Data presented as mean ±SEM, n=3-9. $^{*}p<0.05$, WT vs. D1KO (two-tailed unpaired t-test).

Figure 8: *Tbc1d1/Tbc1d4*-deficiency reduces glycogen content, increases triglyceride levels and abundance of PCK1 and **PCK2 in the liver.** Tissues from 16-week-old male mice were analyzed for content in triglycerides and glycogen, and for protein expression of PCK1 and PCK2 by Western Blot. A, Glycogen content in liver (n=18-24). B, Glycogen content in *Gastrocnemius* muscle (n=7). C, Hepatic triglyceride content (n=12-19). D, Triglyceride content in *Quadriceps* muscle (n=7-13). E, F, Abundance of hepatic PCK1 and PCK2 expression (n=6). Data presented as mean ±SEM. $^{*}p<0.05$, $^{**}p<0.01$, $^{***}p<0.001$, WT vs. D1KO, D4KO, D1/4KO (one-way ANOVA).

References

1. Leto D, Saltiel AR: Regulation of glucose transport by insulin: traffic control of GLUT4. Nature reviews Molecular cell biology 2012;13:383-396
2. Holman GD, Cushman SW: Subcellular localization and trafficking of the GLUT4 glucose transporter isoform in insulin-responsive cells. BioEssays : news and reviews in molecular, cellular and developmental biology 1994;16:753-759
3. Sano H, Kane S, Sano E, Miinea CP, Asara JM, Lane WS, Garner CW, Lienhard GE: Insulin-stimulated phosphorylation of a Rab GTPase-activating protein regulates GLUT4 translocation. J Biol Chem 2003;278:14599-14602
4. Roach WG, Chavez JA, Miinea CP, Lienhard GE: Substrate specificity and effect on GLUT4 translocation of the Rab GTPase-activating protein Tbc1d1. Biochem J 2007;403:353-358
5. Kramer HF, Witczak CA, Fujii N, Jessen N, Taylor EB, Arnolds DE, Sakamoto K, Hirshman MF, Goodyear LJ: Distinct signals regulate AS160 phosphorylation in response to insulin, AICAR, and contraction in mouse skeletal muscle. Diabetes 2006;55:2067-2076
6. Chen S, Murphy J, Toth R, Campbell DG, Morrice NA, Mackintosh C: Complementary regulation of TBC1D1 and AS160 by growth factors, insulin and AMPK activators. Biochem J 2008;409:449-459
7. Sakamoto K, Holman GD: Emerging role for AS160/TBC1D4 and TBC1D1 in the regulation of GLUT4 traffic. Am J Physiol Endocrinol Metab 2008;295:E29-37

8. An D, Toyoda T, Taylor EB, Yu H, Fujii N, Hirshman MF, Goodyear LJ: TBC1D1 regulates insulin- and contraction-induced glucose transport in mouse skeletal muscle. Diabetes 2010;59:1358-1365
9. Funai K, Cartee GD: Inhibition of contraction-stimulated AMP-activated protein kinase inhibits contraction-stimulated increases in PAS-TBC1D1 and glucose transport without altering PAS-AS160 in rat skeletal muscle. Diabetes 2009;58:1096-1104
10. Chadt A, Leicht K, Deshmukh A, Jiang LQ, Scherneck S, Bernhardt U, Dreja T, Vogel H, Schmolz K, Kluge R, Zierath JR, Hultschig C, Hoeben RC, Schurmann A, Joost HG, Al-Hasani H: Tbc1d1 mutation in lean mouse strain confers leanness and protects from diet-induced obesity. Nat Genet 2008;40:1354-1359
11. Stone S, Abkevich V, Russell DL, Riley R, Timms K, Tran T, Trem D, Frank D, Jammulapati S, Neff CD, Iliev D, Gress R, He G, Frech GC, Adams TD, Skolnick MH, Lanchbury JS, Gutin A, Hunt SC, Shattuck D: TBC1D1 is a candidate for a severe obesity gene and evidence for a gene/gene interaction in obesity predisposition. Hum Mol Genet 2006;15:2709-2720
12. Meyre D, Farge M, Lecoeur C, Proenca C, Durand E, Allegaert F, Tichet J, Marre M, Balkau B, Weill J, Delplanque J, Froguel P: R125W coding variant in TBC1D1 confers risk for familial obesity and contributes to linkage on chromosome 4p14 in the French population. Hum Mol Genet 2008;17:1798-1802
13. Dash S, Sano H, Rochford JJ, Semple RK, Yeo G, Hyden CS, Soos MA, Clark J, Rodin A, Langenberg C, Druet C, Fawcett KA, Tung YC, Wareham NJ, Barroso I, Lienhard GE, O'Rahilly S, Savage DB: A truncation mutation in TBC1D4 in a family with acanthosis nigricans and postprandial hyperinsulinemia. Proc Natl Acad Sci U S A 2009;106:9350-9355
14. Wang HY, Ducommun S, Quan C, Xie B, Li M, Wasserman DH, Sakamoto K, Mackintosh C, Chen S: AS160 deficiency causes whole-body insulin resistance via composite effects in multiple tissues. Biochem J 2013;449:479-489
15. Szekeres F, Chadt A, Tom RZ, Deshmukh AS, Chibalin AV, Bjornholm M, Al-Hasani H, Zierath JR: The Rab-GTPase-activating protein TBC1D1 regulates skeletal muscle glucose metabolism. Am J Physiol Endocrinol Metab 2012;303:E524-533
16. Miinea CP, Sano H, Kane S, Sano E, Fukuda M, Peranen J, Lane WS, Lienhard GE: AS160, the Akt substrate regulating GLUT4 translocation, has a functional Rab GTPase-activating protein domain. Biochem J 2005;391:87-93
17. Hatakeyama H, Kanzaki M: Regulatory mode shift of Tbc1d1 is required for acquisition of insulin-responsive GLUT4-trafficking activity. Molecular biology of the cell 2013;24:809-817
18. Koumanov F, Richardson JD, Murrow BA, Holman GD: AS160 phosphotyrosine-binding domain constructs inhibit insulin-stimulated GLUT4 vesicle fusion with the plasma membrane. J Biol Chem 2011;286:16574-16582
19. Tan SX, Ng Y, Burchfield JG, Ramm G, Lambright DG, Stockli J, James DE: The RabGAP TBC1D4/AS160 contains an atypical PTB domain that interacts with plasma membrane phospholipids to facilitate GLUT4 trafficking in adipocytes. Mol Cell Biol 2012;
20. Sun Y, Bilan PJ, Liu Z, Klip A: Rab8A and Rab13 are activated by insulin and regulate GLUT4 translocation in muscle cells. Proc Natl Acad Sci U S A 2010;107:19909-19914
21. Brewer PD, Romenskaia I, Kanow MA, Mastick CC: Loss of AS160 Akt substrate causes Glut4 protein to accumulate in compartments that are primed for fusion in basal adipocytes. J Biol Chem 2011;286:26287-26297
22. Eguez L, Lee A, Chavez JA, Miinea CP, Kane S, Lienhard GE, McGraw TE: Full intracellular retention of GLUT4 requires AS160 Rab GTPase activating protein. Cell Metab 2005;2:263-272

23. Dokas J, Chadt A, Nolden T, Himmelbauer H, Zierath JR, Joost HG, Al-Hasani H: Conventional knockout of Tbc1d1 in mice impairs insulin- and AICAR-stimulated glucose uptake in skeletal muscle. Endocrinology 2013;
24. Lansey MN, Walker NN, Hargett SR, Stevens JR, Keller SR: Deletion of Rab GAP AS160 modifies glucose uptake and GLUT4 translocation in primary skeletal muscles and adipocytes and impairs glucose homeostasis. Am J Physiol Endocrinol Metab 2012;
25. Wakeland E, Morel L, Achey K, Yui M, Longmate J: Speed congenics: a classic technique in the fast lane (relatively speaking). Immunology today 1997;18:472-477
26. Livak KJ, Schmittgen TD: Analysis of relative gene expression data using real-time quantitative PCR and the 2(-Delta Delta C(T)) Method. Methods 2001;25:402-408
27. Peronnet F, Massicotte D: Table of nonprotein respiratory quotient: an update. Can J Sport Sci 1991;16:23-29
28. Passonneau JV, Lauderdale VR: A comparison of three methods of glycogen measurement in tissues. Anal Biochem 1974;60:405-412
29. Gliemann J, Rees WD, Foley JA: The fate of labelled glucose molecules in the rat adipocyte. Dependence on glucose concentration. Biochim Biophys Acta 1984;804:68-76
30. Al-Hasani H, Hinck CS, Cushman SW: Endocytosis of the glucose transporter GLUT4 is mediated by the GTPase dynamin. J Biol Chem 1998;273:17504-17510
31. Hashimoto M, Hatanaka Y, Yang J, Dhesi J, Holman GD: Synthesis of biotinylated bis(D-glucose) derivatives for glucose transporter photoaffinity labelling. Carbohydrate research 2001;331:119-127
32. Keller SR, Scott HM, Mastick CC, Aebersold R, Lienhard GE: Cloning and characterization of a novel insulin-regulated membrane aminopeptidase from Glut4 vesicles. J Biol Chem 1995;270:23612-23618
33. Chen S, Wasserman DH, MacKintosh C, Sakamoto K: Mice with AS160/TBC1D4-Thr649Ala knockin mutation are glucose intolerant with reduced insulin sensitivity and altered GLUT4 trafficking. Cell Metab 2011;13:68-79
34. Rutti S, Arous C, Nica AC, Kanzaki M, Halban PA, Bouzakri K: Expression, phosphorylation and function of the Rab-GTPase activating protein TBC1D1 in pancreatic beta-cells. FEBS Lett 2014;588:15-20
35. Bouzakri K, Ribaux P, Tomas A, Parnaud G, Rickenbach K, Halban PA: Rab GTPase-activating protein AS160 is a major downstream effector of protein kinase B/Akt signaling in pancreatic beta-cells. Diabetes 2008;57:1195-1204
36. Kotani K, Peroni OD, Minokoshi Y, Boss O, Kahn BB: GLUT4 glucose transporter deficiency increases hepatic lipid production and peripheral lipid utilization. J Clin Invest 2004;114:1666-1675
37. Seixas E, Barros M, Seabra MC, Barral DC: Rab and Arf proteins in genetic diseases. Traffic 2013;14:871-885
38. Ross SA, Herbst JJ, Keller SR, Lienhard GE: Trafficking kinetics of the insulin-regulated membrane aminopeptidase in 3T3-L1 adipocytes. Biochem Biophys Res Commun 1997;239:247-251
39. Malide D, St-Denis JF, Keller SR, Cushman SW: Vp165 and GLUT4 share similar vesicle pools along their trafficking pathways in rat adipose cells. FEBS Lett 1997;409:461-468
40. Peck GR, Ye S, Pham V, Fernando RN, Macaulay SL, Chai SY, Albiston AL: Interaction of the Akt substrate, AS160, with the glucose transporter 4 vesicle marker protein, insulin-regulated aminopeptidase. Molecular endocrinology 2006;20:2576-2583
41. Jordens I, Molle D, Xiong W, Keller SR, McGraw TE: Insulin-regulated aminopeptidase is a key regulator of GLUT4 trafficking by controlling the sorting of GLUT4 from endosomes to specialized insulin-regulated vesicles. Molecular biology of the cell 2010;21:2034-2044
42. Al-Hasani H, Yver DR, Cushman SW: Overexpression of the glucose transporter GLUT4 in adipose cells interferes with insulin-stimulated translocation. FEBS Lett 1999;460:338-342

43. Zisman A, Peroni OD, Abel ED, Michael MD, Mauvais-Jarvis F, Lowell BB, Wojtaszewski JF, Hirshman MF, Virkamaki A, Goodyear LJ, Kahn CR, Kahn BB: Targeted disruption of the glucose transporter 4 selectively in muscle causes insulin resistance and glucose intolerance. Nat Med 2000;6:924-928
44. Abel ED, Peroni O, Kim JK, Kim YB, Boss O, Hadro E, Minnemann T, Shulman GI, Kahn BB: Adipose-selective targeting of the GLUT4 gene impairs insulin action in muscle and liver. Nature 2001;409:729-733
45. Ren JM, Marshall BA, Mueckler MM, McCaleb M, Amatruda JM, Shulman GI: Overexpression of Glut4 protein in muscle increases basal and insulin-stimulated whole body glucose disposal in conscious mice. J Clin Invest 1995;95:429-432
46. Ishikura S, Klip A: Muscle cells engage Rab8A and myosin Vb in insulin-dependent GLUT4 translocation. American journal of physiology Cell physiology 2008;295:C1016-1025
47. Kim YB, Peroni OD, Aschenbach WG, Minokoshi Y, Kotani K, Zisman A, Kahn CR, Goodyear LJ, Kahn BB: Muscle-specific deletion of the Glut4 glucose transporter alters multiple regulatory steps in glycogen metabolism. Mol Cell Biol 2005;25:9713-9723
48. Stockli J, Fazakerley DJ, James DE: GLUT4 exocytosis. J Cell Sci 2011;124:4147-4159
49. Kaddai V, Le Marchand-Brustel Y, Cormont M: Rab proteins in endocytosis and Glut4 trafficking. Acta physiologica 2008;192:75-88
50. Sun Y, Chiu TT, Foley KP, Bilan PJ, Klip A: Myosin Va mediates Rab8A-regulated GLUT4 vesicle exocytosis in insulin-stimulated muscle cells. Molecular biology of the cell 2014;
51. Chen Y, Wang Y, Zhang J, Deng Y, Jiang L, Song E, Wu XS, Hammer JA, Xu T, Lippincott-Schwartz J: Rab10 and myosin-Va mediate insulin-stimulated GLUT4 storage vesicle translocation in adipocytes. The Journal of cell biology 2012;198:545-560
52. Reed SE, Hodgson LR, Song S, May MT, Kelly EE, McCaffrey MW, Mastick CC, Verkade P, Tavare JM: A role for Rab14 in the endocytic trafficking of GLUT4 in 3T3-L1 adipocytes. J Cell Sci 2013;126:1931-1941
53. Sadacca LA, Bruno J, Wen J, Xiong W, McGraw TE: Specialized sorting of GLUT4 and its recruitment to the cell surface are independently regulated by distinct Rabs. Molecular biology of the cell 2013;24:2544-2557

Figure 1

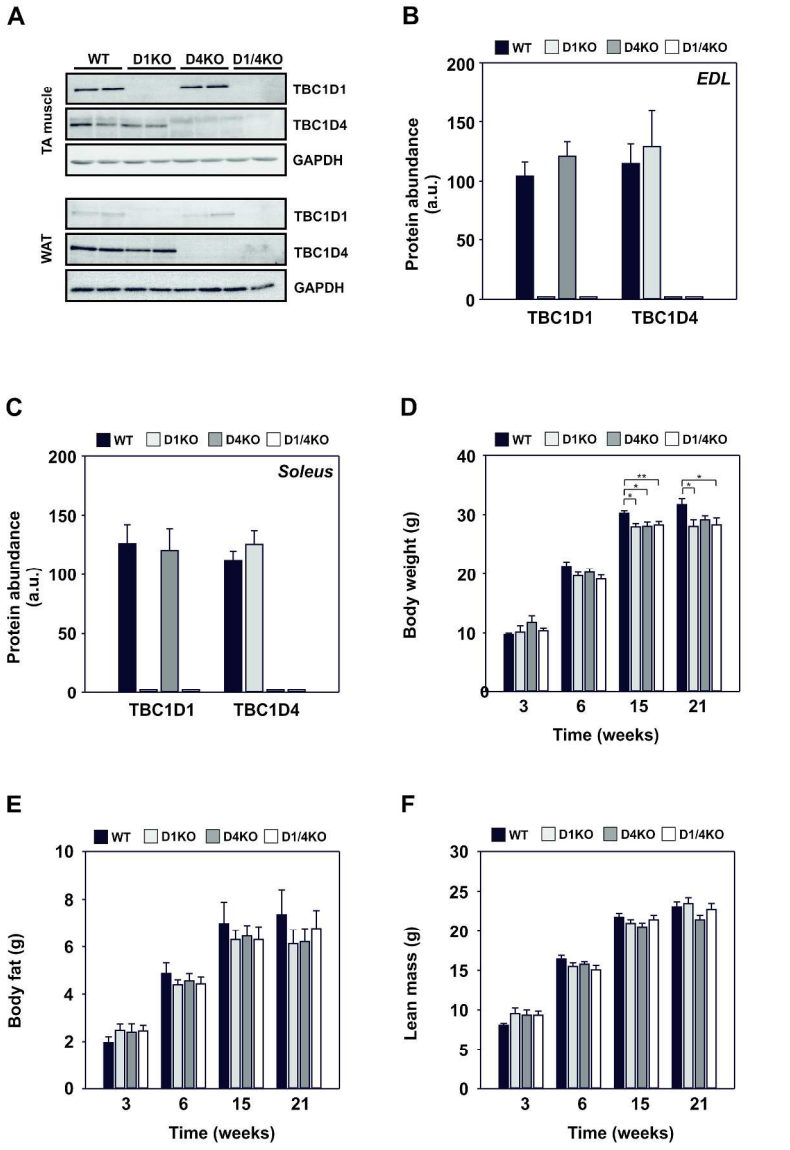

273x388mm (300 x 300 DPI)

Figure 2

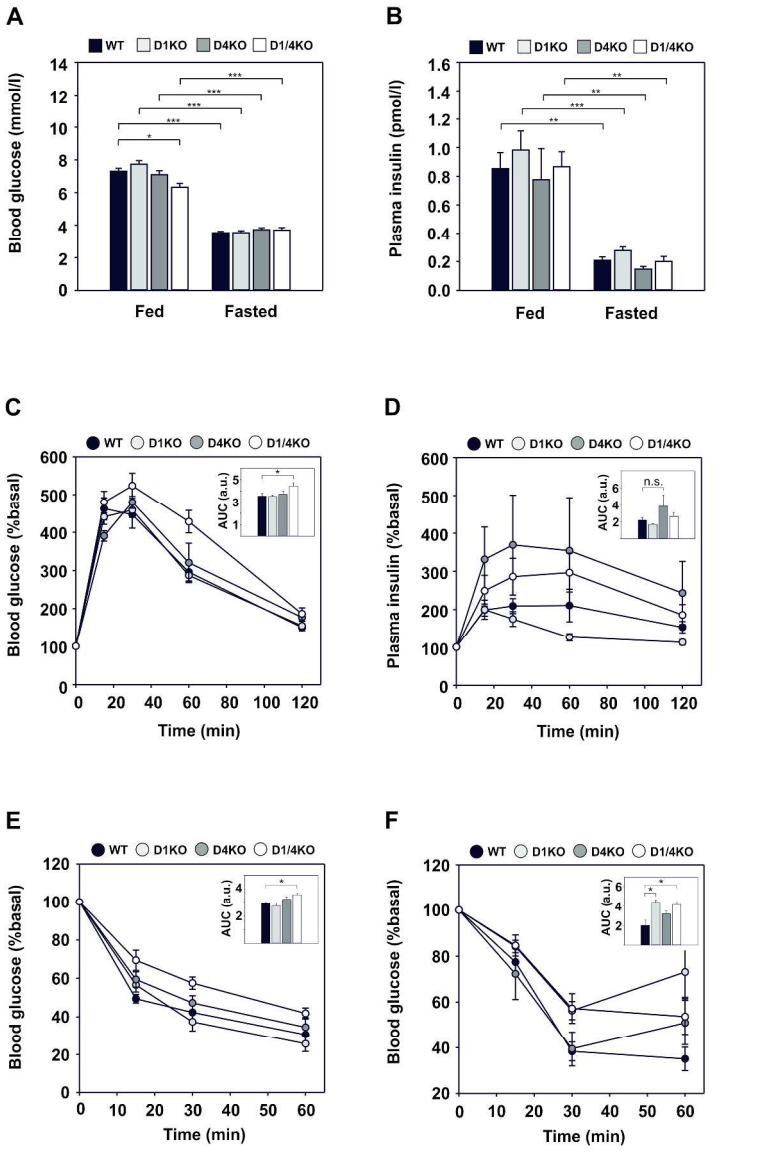

283x422mm (300 x 300 DPI)

Figure 3

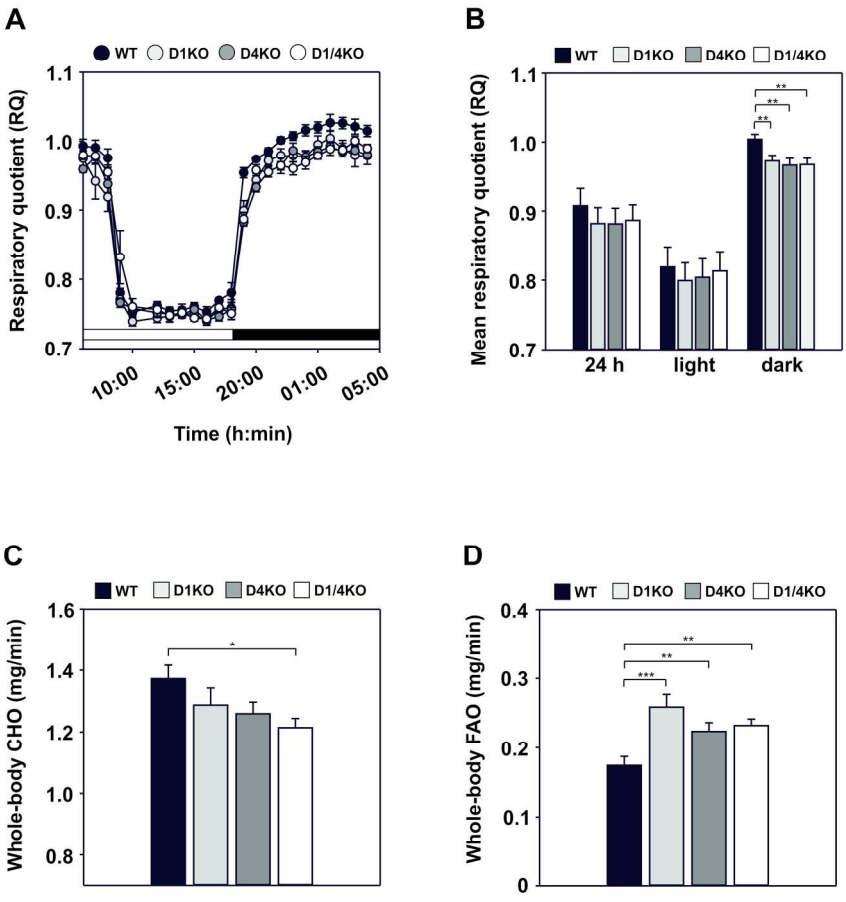

190x185mm (300 x 300 DPI)

Figure 4

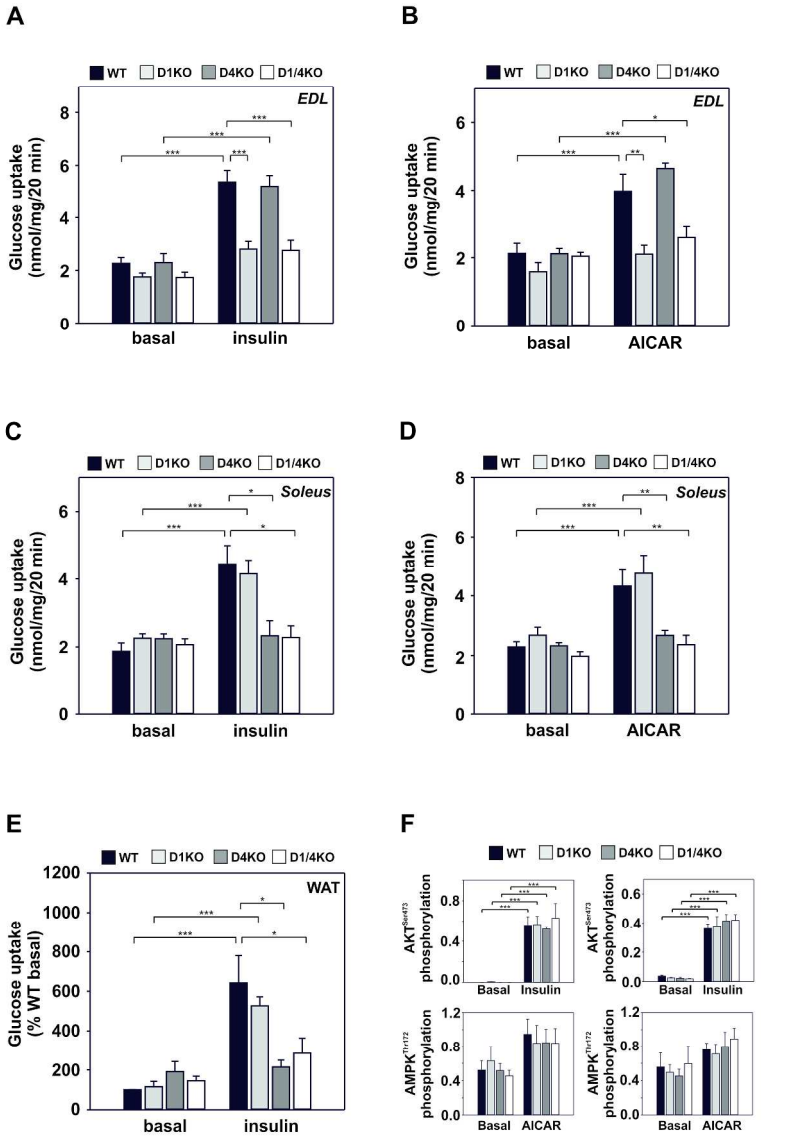

273x382mm (300 x 300 DPI)

Figure 5

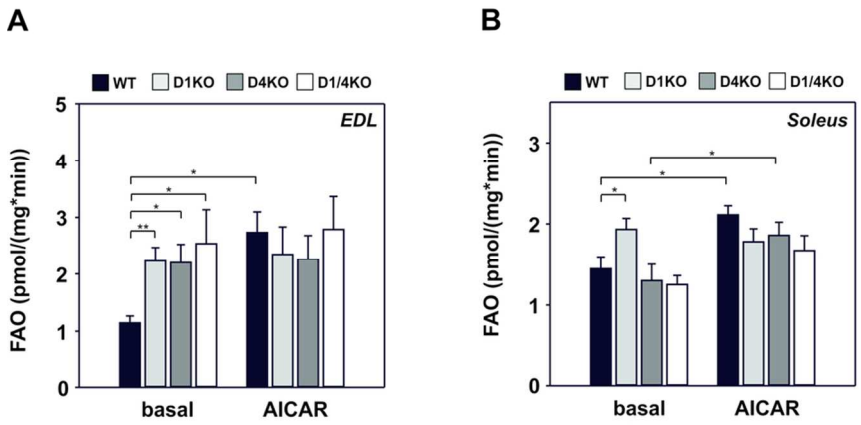

94x46mm (300 x 300 DPI)

Figure 6

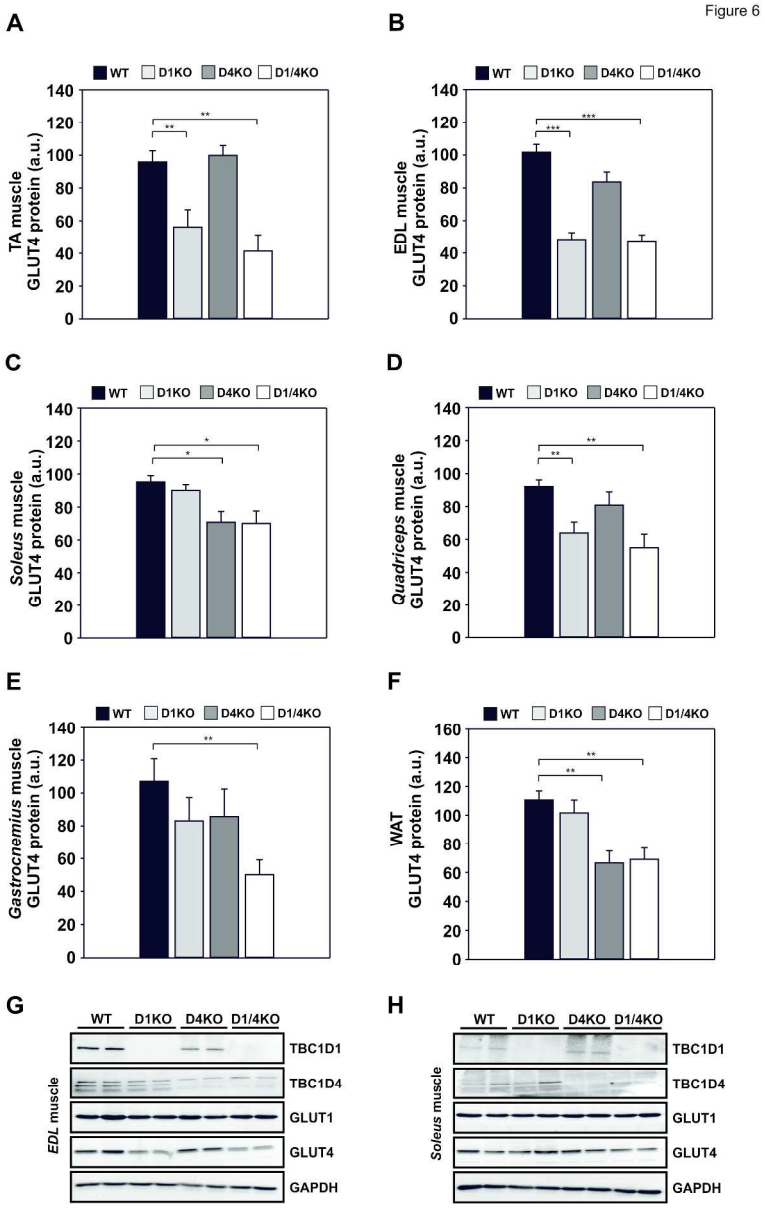

282x407mm (300 x 300 DPI)

Figure 7

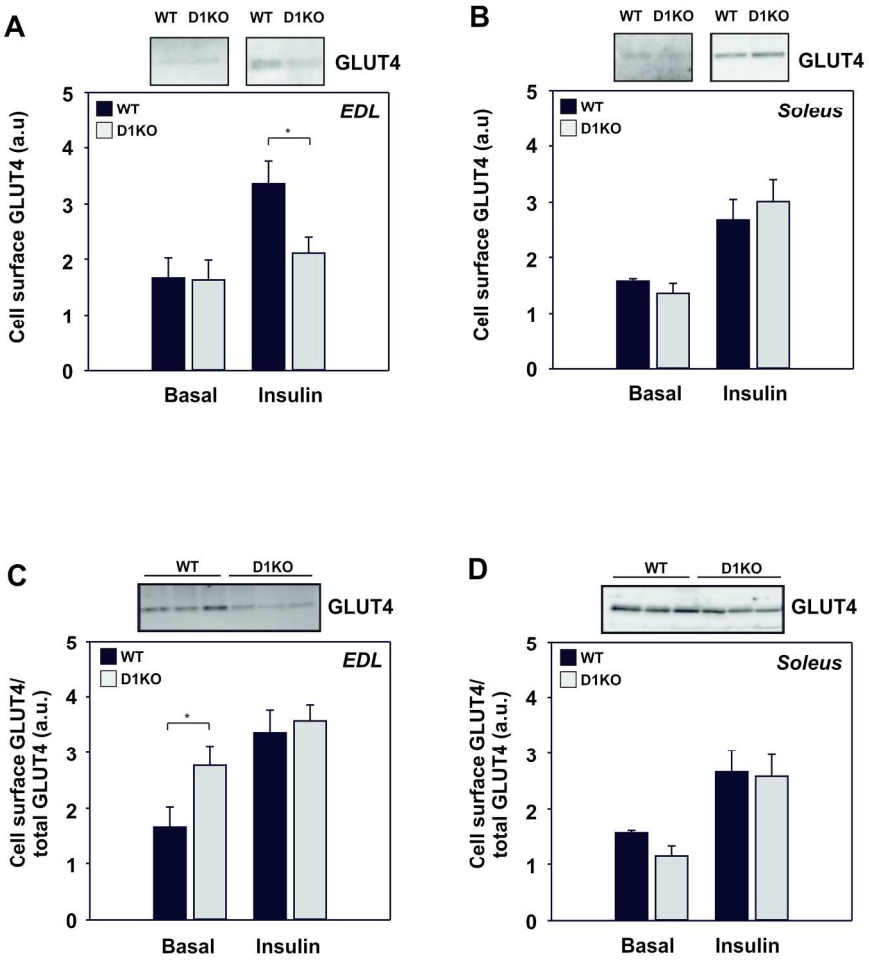

207x221mm (300 x 300 DPI)

Figure 8

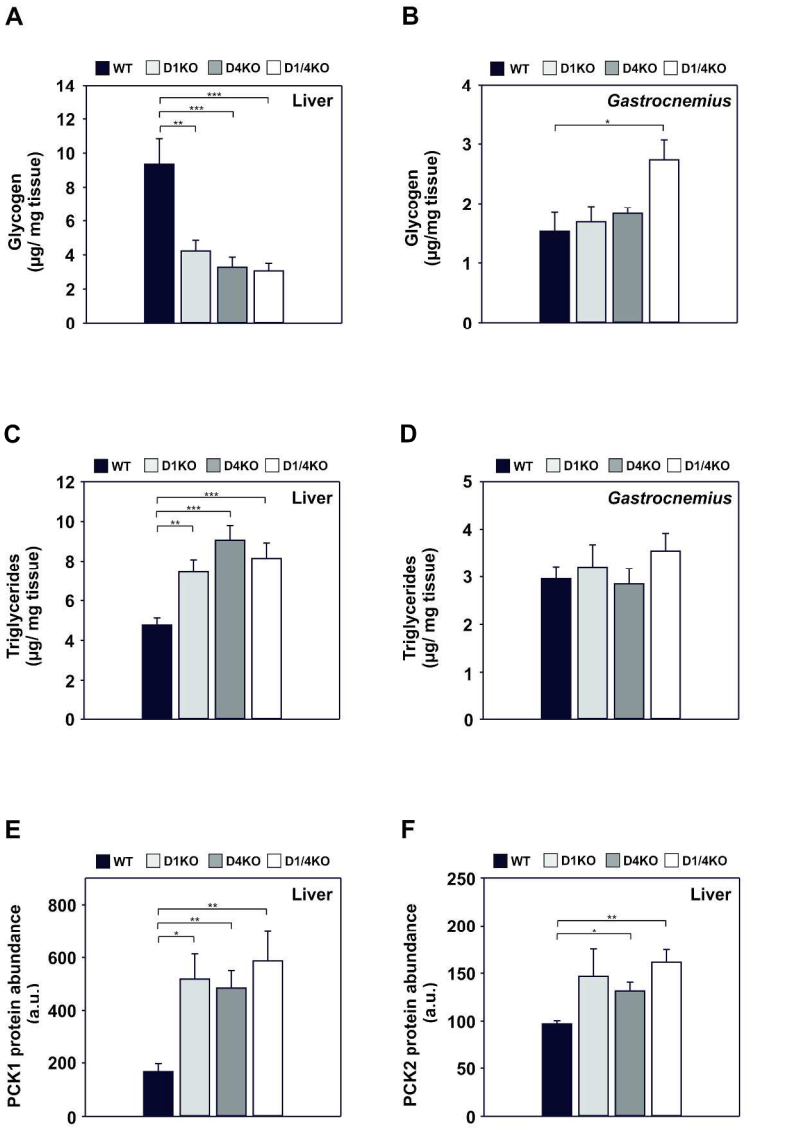

271x378mm (300 x 300 DPI)

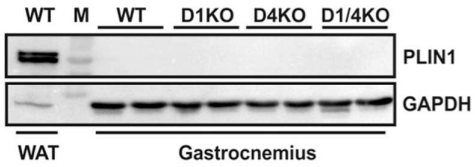

Online Supplementary Figure 1: Western blot analysis of Perilipin 1 (PLIN1) protein abundance in Gastrocnemius muscle homogenates from wildtype (WT), *Tbc1d1*-deficient (D1KO), *Tbc1d4*-deficient (D4KO) and double-deficient (D1/4KO) mice. Tissue homogenates for triglyceride analysis were tested for contamination with adipose cells. GAPDH served as loading control. Protein load: 40 μg/lane. WAT, white adipose tissue; M, Molecular mass marker.

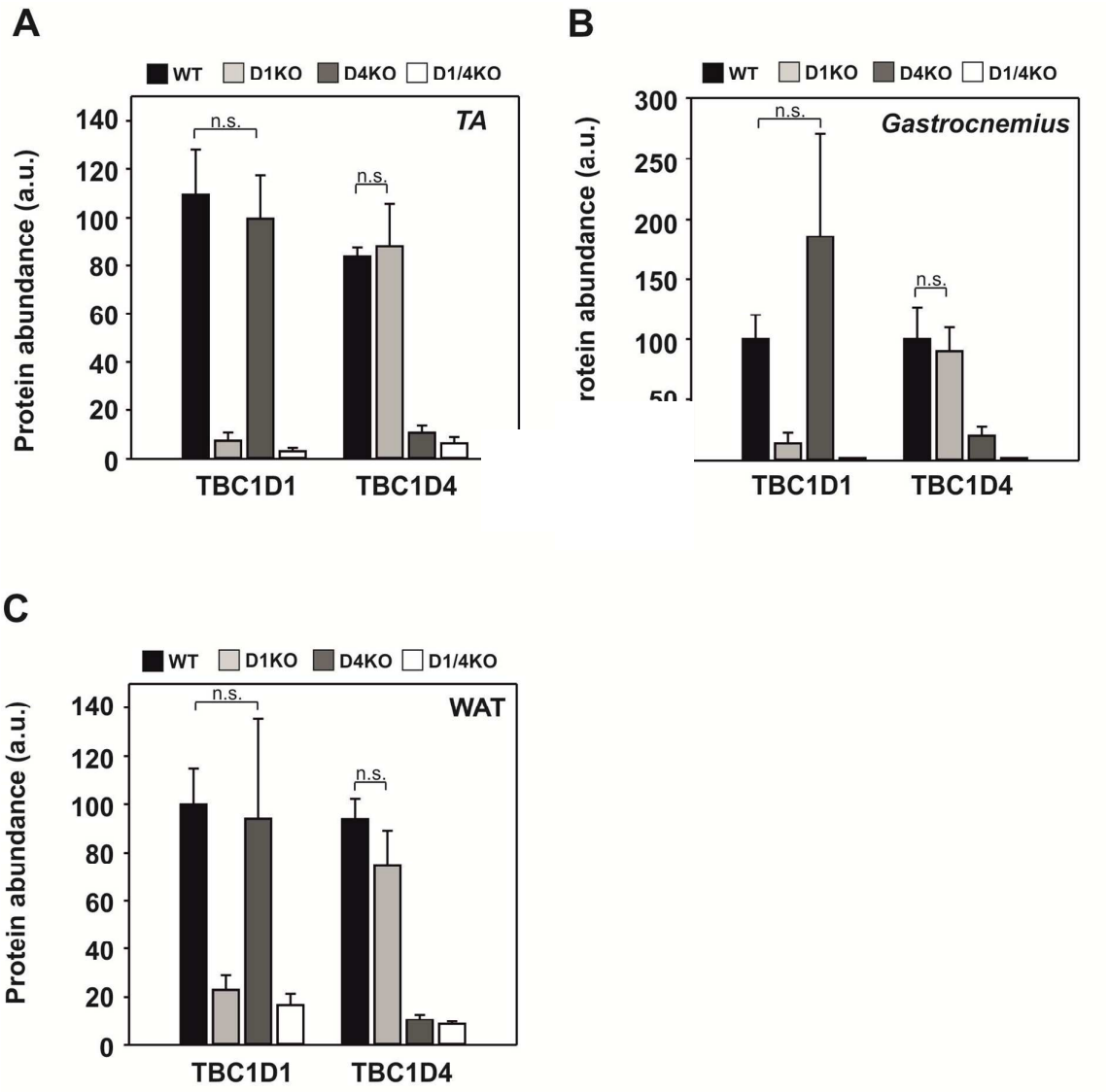

Online Supplementary Figure 2: Abundance of TBC1D1 and TBC1D4 in skeletal muscle and white adipose tissue (WAT) from wildtype (WT), *Tbc1d1*-deficient (D1KO), *Tbc1d4*-deficient (D4KO) and double-deficient (D1/4KO) mice. Protein lysates from *Gastrocnemius* muscle (A), *TA* (*Tibialis anterior*) muscle (B) and white adipose tissue (WAT) (C) of WT, D1KO, D4KO and D1/4KO male mice were prepared and subjected to Western Blot analysis of TBC1D1 and TBC1D4. Data presented as mean ±SEM, n=3-6. N.s., not statistically significant, WT vs. D1KO, D4KO (one-way ANOVA).

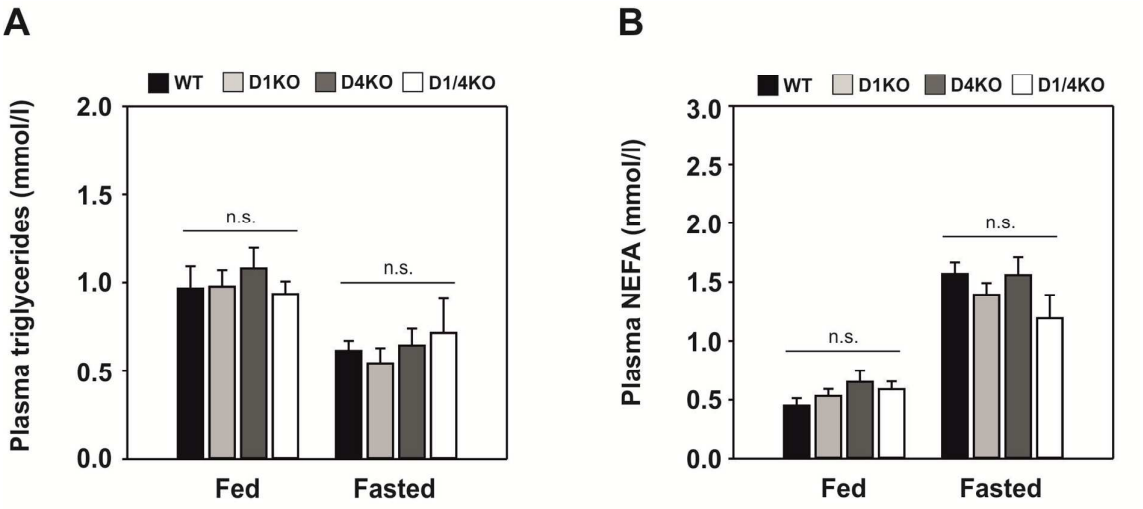

Online Supplementary Figure 3: Plasma lipids in wildtype (WT), *Tbc1d1*-deficient (D1KO), *Tbc1d4*-deficient (D4KO) and double-deficient (D1/4KO) mice. Plasma from randomly fed and 6h-fasted 17-23 weeks old male mice on standard diet was analyzed for triglyceride content (A) and amount of non-esterified free fatty acids (NEFAs) (B) using the Serum Triglyceride Determination Kit (Sigma-Aldrich, Catalog Number TR0100) and the NEFA-HR (2) system (Wako Chemicals, Neuss, Germany) according to the manufacturer`s instructions, respectively. Data are presented as mean ±SEM, n=6-12. N.s., not statistically significant, WT vs. D1KO, D4KO, D1/4KO (one-way ANOVA).

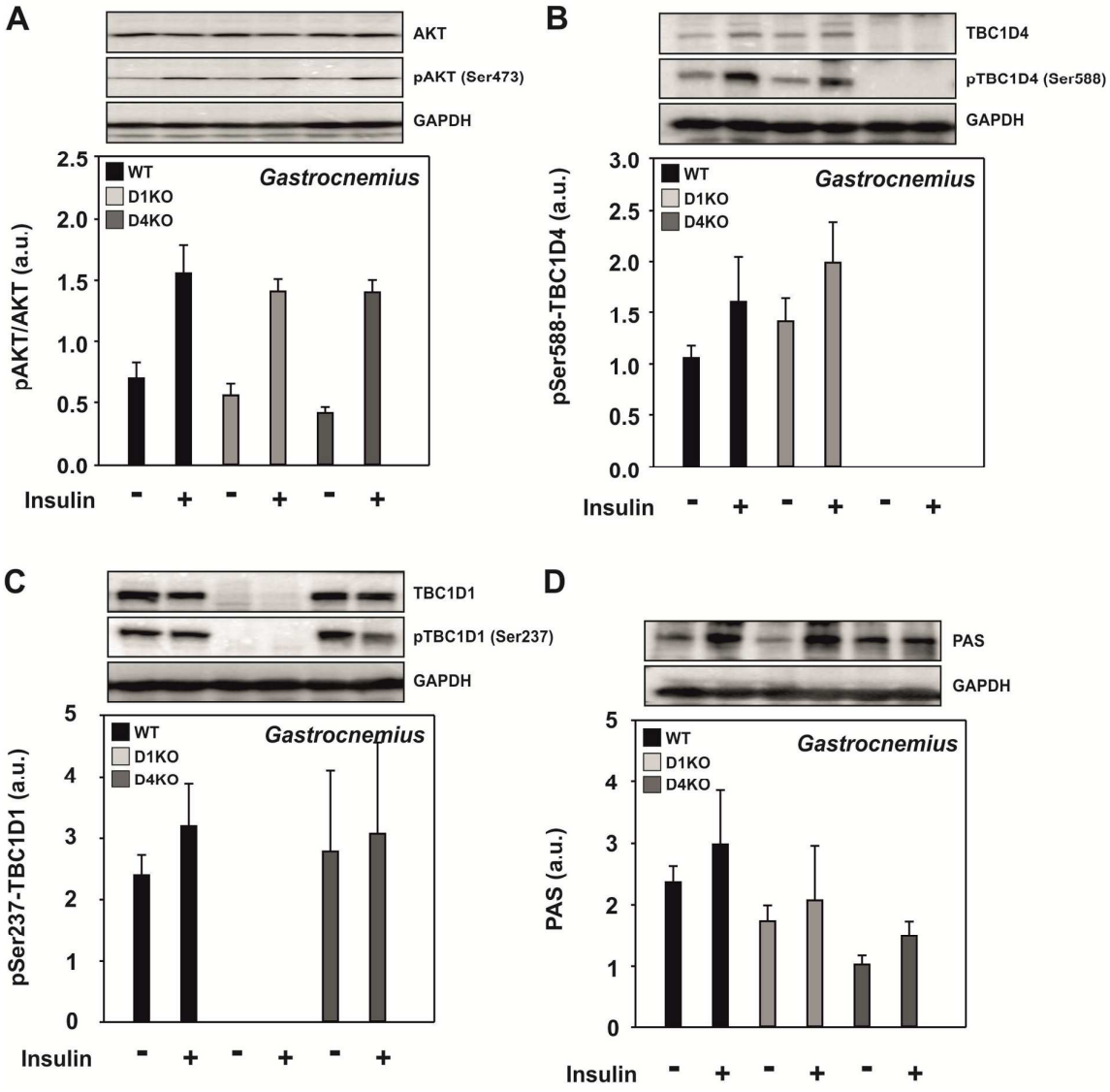

Online Supplementary Figure 4: Analysis of TBC1D1 and TBC1D4 phosphorylation in Gastrocnemius muscle from *in vivo* insulin-stimulated wildtype (WT), *Tbc1d1*-deficient (D1KO) and *Tbc1d4*-deficient (D4KO) mice. Mice were i.p. injected with 1 IU/kg Insulin and sacrificed by cervical dislocation after 10 minutes. Tissues were removed and immediately frozen in liquid nitrogen. Protein lysates from stimulated and unstimulated (i.p. injection of 0.9% saline solution) skeletal muscles were prepared and subjected to Western Blot analysis of AKT phosphorylation, $pSer^{588}$-TBC1D4, $pSer^{237}$-TBC1D1 and 'Phosphorylated AKT substrate' (PAS). Data presented as mean ±SEM, n=3.

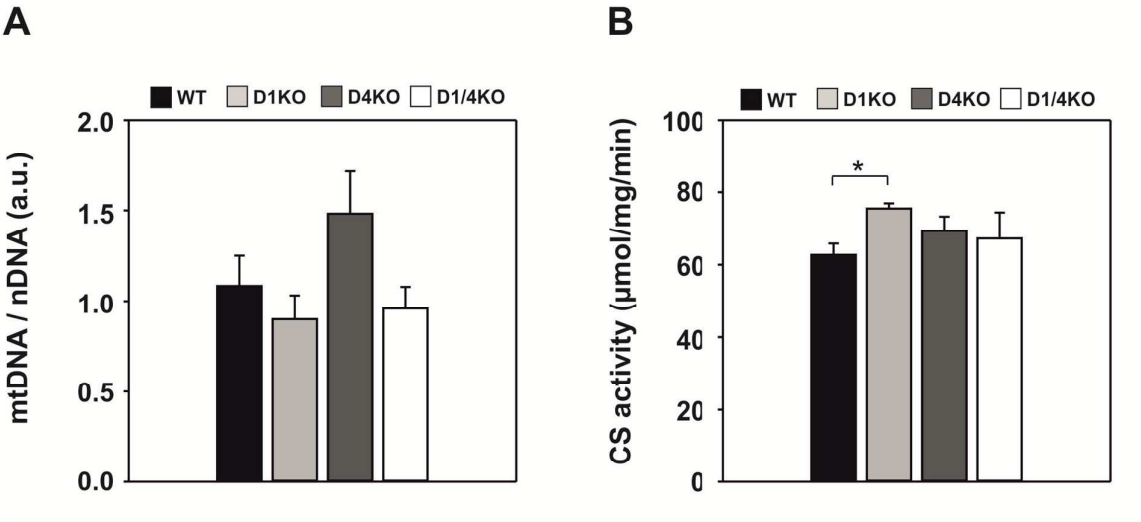

Online Supplementary Figure 5: Mitochondrial copy number and citrate synthase activity in *Gastrocnemius* muscle from wildtype (WT), *Tbc1d1*-deficient (D1KO), *Tbc1d4*-deficient (D4KO) and double-deficient (D1/4KO) mice. A) Mitochondrial copy number. The ratio of mtDNA (mt-Nd2) and nuclear DNA (18S) was determined by quantitative Realtime PCR using SYBR-Green. B) Citrate synthase activity was analyzed in protein lysates using the Citrate Synthase Assay Kit (Sigma-Aldrich, Catalog Number CS0720) according to the manufacturer`s instructions. All analyses were performed as described in Dokas et al., 2013 (Endocrinology 154:3502–3514). Data presented as mean ±SEM, n=8. *p<0.05, WT vs. D1KO (one-way ANOVA).

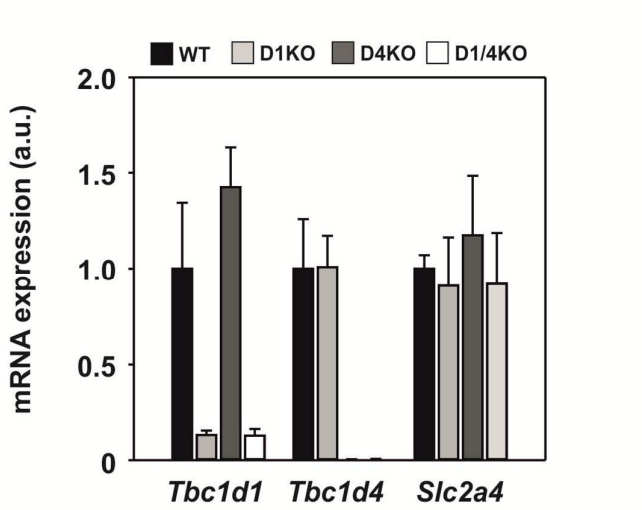

Online Supplementary Figure 6: mRNA expression of RabGAP and GLUT4 genes in *Tibialis anterior* (*TA*) muscle from wildtype (WT), *Tbc1d1*-deficient (D1KO), *Tbc1d4*-deficient (D4KO) and double-deficient (D1/4KO) mice. Expression levels were determined by quantitative Realtime PCR analysis using TaqMan PCR probes (Applied Biosystems, Foster City, USA) for *Tbc1d1* (Mm00497989_m1), *Tbc1d4* (Mm00557659_m1), and *Slc2a4* (Mm00436615_m1). Data were normalized to *Actb* (Mm00607939). Data presented as mean ±SEM, n=6.

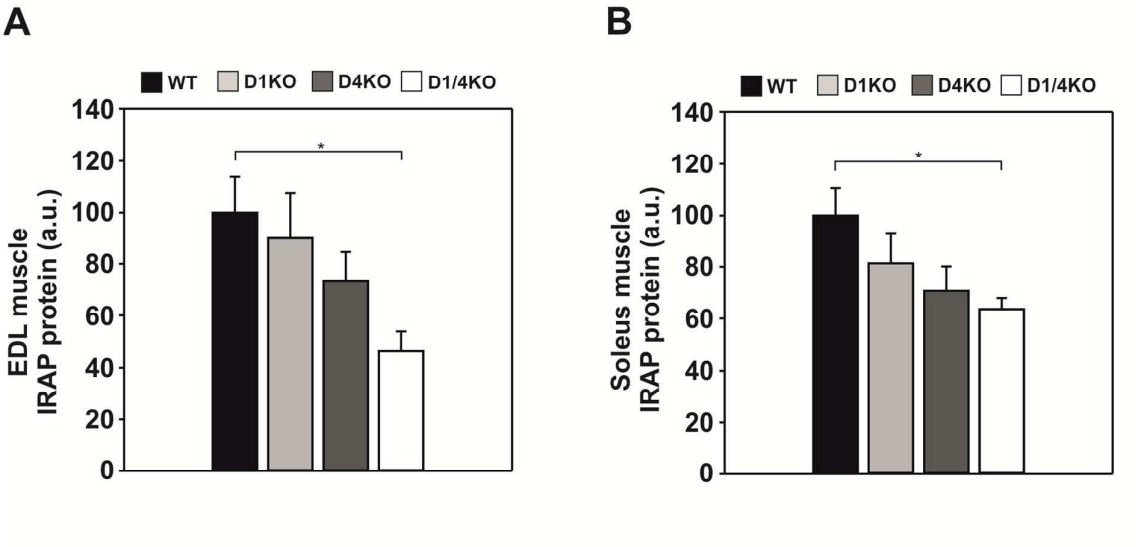

Online Supplementary Figure 7: IRAP protein abundance in skeletal muscle from wildtype (WT), *Tbc1d1*-deficient (D1KO), *Tbc1d4*-deficient (D4KO) and double-deficient (D1/4KO) mice. Protein lysates from A) *Extensor digitorum longus* (EDL) and B) *Soleus* muscles were analyzed by Western Blot for IRAP protein. Data presented as mean ±SEM, n=6. *p<0.05, WT vs. D4KO (one-way ANOVA).

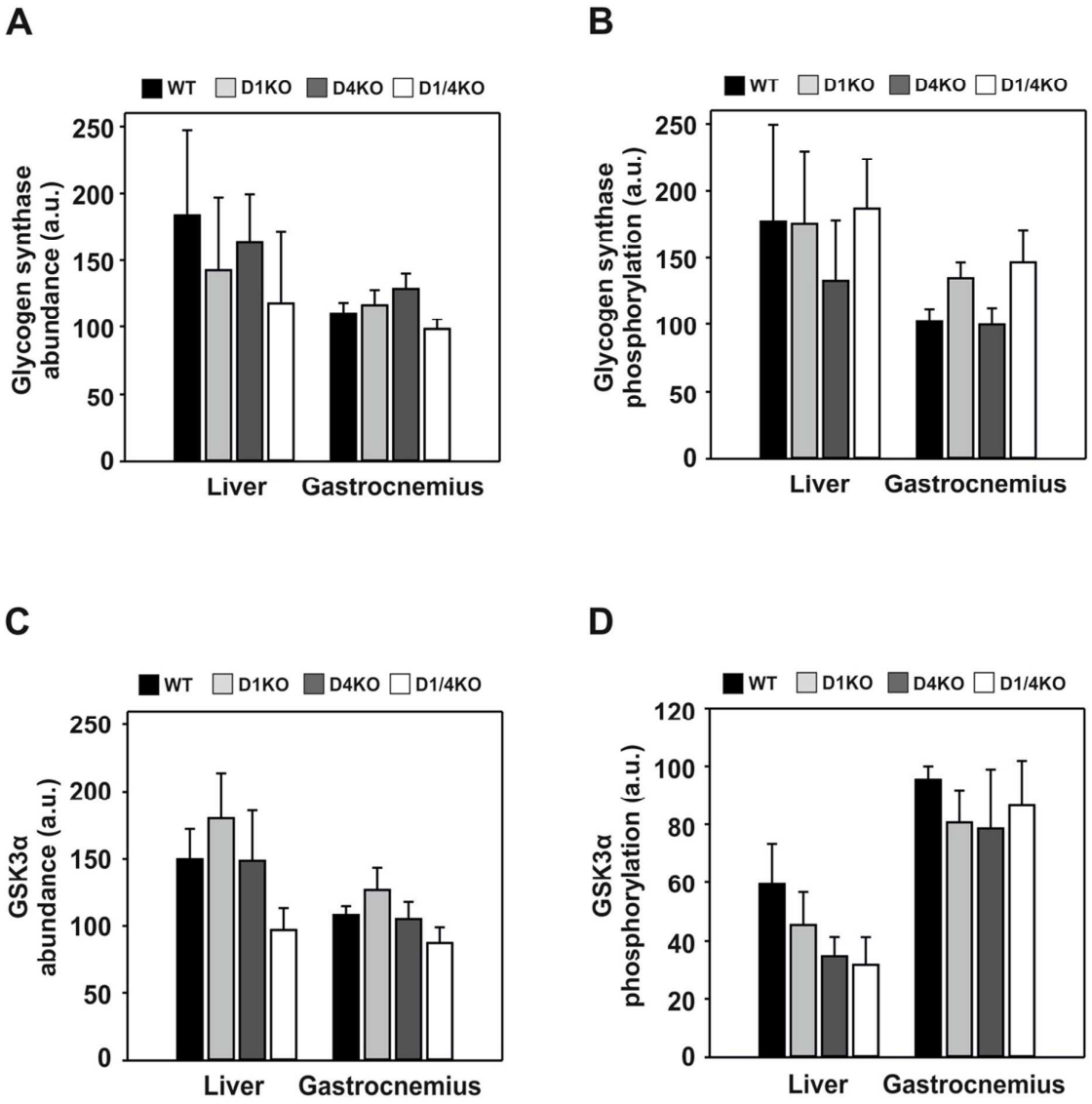

Online Supplementary Figure 8: Abundance of glycogen synthase (GS) and glycogen synthase kinase 3 α (GSK3α), and phosphorylation of GS and GSK3α in liver and skeletal muscle from wildtype (WT), *Tbc1d1*-deficient (D1KO) and *Tbc1d4*-deficient (D4KO) and double-deficient (D1/4KO) mice. Protein lysates from liver and Gastrocnemius muscle of WT, D1KO, D4KO and D1/4KO male mice were prepared and subjected to Western Blot analysis. A) GS, B) Phospho-GS (Ser^{641}), C), GSK3α and D), Phospho-GSK3α (Ser^{21}). Data presented as mean ±SEM, n=6.